Sherman, G., & Folch-Pi, J. (1970) *J. Neurochem. 17*, 597.
Spiker, R. C., & Levin, I. W. (1976) *Biochim. Biophys. Acta 455*, 560.
Verma, S. P., Wallach, D. F. H., & Sakura, J. D. (1980) *Biochemistry 19*, 574.
Wu, E.-S., Jacobsin, K., & Papahadjopoulous, D. (1977) *Biochemistry 16*, 3936.
Yellin, N., & Levin, I. W. (1977a) *Biochemistry 16*, 642.
Yellin, N., & Levin, I. W. (1977b) *Biochim. Biophys. Acta 489*, 177.

Comparative Lateral Diffusion of Fluorescent Lipid Analogues in Phospholipid Multibilayers†

Zenon Derzko‡ and Kenneth Jacobson*,‡

ABSTRACT: The method of fluorescence recovery after photobleaching (FRAP) has been used to measure the lateral diffusion coefficient (D) of the following fluorescent lipid probes in lipid multibilayers: carbocyanine dyes with fatty acid chains varying from 6 to 18 carbon atoms; fluorescently labeled phosphatidylcholine, phosphatidylethanolamine, and lysophosphatidylethanolamine; and fluorescently labeled fatty acid derivatives. Measurements were made in dimyristoylphosphatidylcholine (DMPC), dipalmitoylphosphatidylcholine (DPPC), brain phosphatidylserine (PS), and egg phosphatidylcholine (EPC) multibilayers. In the fluid state ($T > T_m$), the diffusion coefficients are relatively insensitive to the structure of the lipid analogue, probably because, if the probe is disposed as an amphipath, its motion depends on the self-diffusion of the host bilayer lipids. The activation energy for the diffusion of most lipid analogues was between 4 and 8 kcal/mol. Significant differences in the lateral diffusion of the analogues were found when bilayers of different composition were compared at the same reduced temperature. Diffusion in longer chain natural phospholipid (EPC, PS) bilayers was significantly slower than in shorter chain saturates (DMPC, DPPC). On the other hand, diffusion in DPPC bilayers was faster than in DMPC membranes which correlates with the greater lateral expansion of DPPC compared to DMPC bilayers above their respective transitions [Janiak, M., Small, D., & Shipley, C. G. (1979) *J. Biol. Chem. 254*, 6068]. Below the transition temperature of DMPC and PS multibilayers, the FRAP kinetics are generally best fitted by two diffusion coefficients. The slow component ($D \leq 5 \times 10^{-11}$ cm^2/s) may be true bulk gel-phase lateral diffusion while the fast component ($10^{-10} < D \lesssim 10^{-8}$ cm^2/s) may be associated with transport along numerous defects apparent in the gel phase. The proportion of fast and slow diffusing probe depends on the structure of the lipid analogue and the chromophore.

The fluorescence recovery after photobleaching (FRAP)[1] technique for measuring the mobility of various fluorescent membrane associated molecules has become a more common experimental procedure. A number of studies have been carried out on lipid and protein diffusion in model membrane systems and directly on single living cells [for review, see Cherry (1979); Jacobson (1980)]. The model-system studies can be used to assist in the interpretation of the results obtained from the cell surface. Recently, fluorescent lipid diffusion has been investigated in multibilayers (Wu et al., 1977; Fahey & Webb, 1978; Smith & McConnell, 1978; Rubenstein et al., 1979), unilamellar vesicles (Fahey & Webb, 1978), and black lipid membranes (Fahey & Webb, 1978). Peptides (Wu et al., 1978), stearoylated dextrans (Wolf et al., 1977), and proteins (Derzko & Jacobson, 1978; Vaz et al., 1978; Smith et al., 1979) have been incorporated into lipid membranes and their diffusions measured.

The purpose of this work was to further study the dependence of lipid analogue diffusion on molecular size and shape in multibilayers composed of several different phospholipids. Comparisons of the diffusion of various probes were made in multibilayers in both the liquid crystalline and the gel phases. A light microscopic study of bilayers undergoing the gel to liquid-crystalline phase transition is also presented.

Materials and Methods

Preparation of Lipids. The phospholipids used in this study were isolated or synthesized by Mr. T. Isac in the laboratory of Dr. D. Papahadjopoulos and contained no detectable impurities as determined by thin-layer chromatography on silica gel H and a solvent of chloroform/methanol/7 M ammonia

† From the Department of Experimental Pathology, Roswell Park Memorial Institute, Buffalo, New York 14263 (K.J.), and the Department of Biophysical Sciences, State University of New York at Buffalo, Buffalo, New York 14226 (Z.D.). *Received March 7, 1980; revised manuscript received July 23, 1980.* This work was supported by Grant CA-16743 awarded by the National Institutes of Health, Department of Health, Education and Welfare. This work was submitted by Z.D. in partial fulfillment of the requirements for the Ph.D. degree at the State University of New York in Buffalo, NY 14226. K.J. is an Established Investigator of the American Heart Association. A preliminary account of this work was presented to the 1979 Biophysical Society Meeting (Derzko & Jacobson, 1979).

‡ Present address: Laboratories for Cell Biology, Department of Anatomy, University of North Carolina, Chapel Hill, NC 27514.

[1] Abbreviations used: DMPC, dimyristoylphosphatidylcholine; DPPC, dipalmitoylphosphatidylcholine; PS, phosphatidylserine; EPC, egg phosphatidylcholine; NBD-PE, *N*-(4-nitrobenzo-2-oxa-1,3-diazolyl)-phosphatidylethanolamine; NBD-PC, 1-acyl-2-[*N*-(4-nitrobenzo-2-oxa-1,3-diazolyl)aminocaproyl]phosphatidylcholine; NBD-lysoPE, *N*-(4-nitrobenzo-2-oxa-1,3-diazolyl)lysophosphatidylethanolamine; NBD-C_{12}, 12-[methyl(7-nitrobenz-2-oxa-1,3-diazol-4-yl)amino]dodecanoic acid; F-C_{16}, 5-(hexadecanoylamino)fluorescein; F-C_{14}, 5-(tetradecanoylamino)fluorescein; diO-C_{18}(3), 3,3′-dioctadecyloxacarbocyanine iodide; diO-C_{14}(3), 3,3′-ditetradecyloxacarbocyanine iodide; diO-C_{10}(3), 3,3′-didecanoyloxacarbocyanine iodide; diO-C_6(3), 3,3′-dihexyloxacarbocyanine iodide; diI-C_{18}(3), 3,3′-dioctadecylindocarbocyanine iodide; diI-C_{16}(3) 3,3′-dihexadecylindocarbocyanine iodide; diI-C_{12}(3),3,3′-didodecanoylindocarbocyanine iodide; T_m, gel to liquid crystalline phase transition temperature; FRAP, fluorescence recovery after photobleaching; % R, percent recovery; $\tau_{1/2}$, half-time for recovery; w_s, laser spot radius at specimen plane; T_B, time of photobleaching; I_B, photobleaching intensity; D, diffusion coefficient.

0006-2960/80/0419-6050$01.00/0

(230:90:15, v/v/v). Dipalmitoylphosphatidylcholine (1,2-dihexadecyl-*sn*-glycero-3-phosphorylcholine, DPPC) and dimyristoylphosphatidylcholine (1,2-ditetradecyl-*sn*-glycero-3-phosphorylcholine, DMPC) were synthesized according to Robles & Van Den Berg (1969) and purified on a silicic acid column. The analysis of fatty acid esters indicated more than 99% palmitic acid and myristic acid for DPPC and DMPC, respectively. Alternatively, A grade DMPC was purchased in crystalline form from Calbiochem, La Jolla, CA. Phosphatidylcholine (EPC) was extracted from egg yolk and phosphatidylserine (PS) was isolated from bovine brain as previously described (Papahadjopoulos & Miller, 1967). The phospholipids were stored at −50 °C as solutions in chloroform (10–20 μmol/mL) in ampules sealed under nitrogen.

Fluorescent Probes and Other Chemicals. The fluorescent dyes 3,3′-dioctadecyloxacarbocyanine iodide [diO-C_{18}(3)], 3,3′-ditetradecyloxacarbocyanine iodide [diO-C_{14}(3)], 3,3′-didecanoyloxacarbocyanine iodide [diO-C_{10}(3)], 3,3′-dihexyloxacarbocyanine iodide [diO-C_6(3)], 3,3′-dioctadecylindocarbocyanine iodide [diI-C_{18}(3)], 3,3′-dihexadecylindocarbocyanine iodide [diI-C_{16}(3)], and 3,3′-didodecanoylindocarbocyanine iodide [diI-C_{12}(3)] were a generous gift of Dr. A. S. Waggoner. The fluorescent fatty acids 12-[methyl-(7-nitrobenz-2-oxa-1,3-diazol-4-yl)-amino]dodecanoic acid (NBD-C_{12}) and 5-(hexadecanoylamino)fluorescein (fluorescein palmitate; F-C_{16}) were obtained from Molecular Probes, Inc. (Plano, TX); 5-(tetradecanoylamino)fluorescein (fluorescein myristate; F-C_{14}) was a generous gift of Dr. F. Szoka. *N*-4-Nitrobenzo-2-oxa-1,3-diazolyl)phosphatidylethanolamine (NBD-PE) and 1-acyl-2-[*N*-(4-nitrobenzo-2-oxa-1,3 diazolyl)aminocaproyl]phosphatidylcholine (NBD-PC), both derived from EPC, were obtained from Avanti Biochemicals, Inc. (Birmingham, AL). All of the carbocyanine dyes, the fluorescein conjugated fatty acids, NBD-C_{12}, NBD-PE, and NBD-PC were >99% pure by thin-layer chromatography as described above.

N-(4-Nitrobenzo-2-oxa-1,3-diazolyl)lysophosphatidylethanolamine (NBD-lysoPE) was prepared in the following manner. Lysophosphatidylethanolamine (lysoPE), purchased from Sigma Chemical Co. (St. Louis, MO), was labeled with NBD-Cl (Pierce Chemical Co., Rockford, IL). About 50 μmol/mL lysoPE was dissolved in tetrahydrofuran with an equimolar amount of triethylamine, to which excess NBD-Cl was added, and the mixture was allowed to react for 1 h at room temperature; the reaction was stopped by adding 10 mL of a citric acid/citrate aqueous buffer which lowered the pH to ~5. Following addition of 70 mL of chloroform, a three-phase system formed. The aqueous phase was decanted, and methanol was added to the remaining emulsion and organic phase until a clear, two-phase system separated. The organic phase was evaporated and the product redissolved in chloroform with anhydrous Na_2SO_4 as a dehydrating agent. After filtration, the product was further purified by preparative thin-layer chromatography using chloroform/methanol/7 M ammonia (230:90:15, v/v/v).

All solvents and chemicals used were reagent grade. Water was twice distilled, the second time in all-glass apparatus.

Lipid Multibilayers and FRAP Measurements. The preparation of fully hydrated lipid multibilayer samples was described previously (Wu et al., 1977). The various fluorescent probe stock solutions in ethanol were premixed with phospholipid solutions in chloroform in concentrations such that the lipid/dye ratios were between 5000 and 10000.

The instrument used for the FRAP experiments was described in detail previously (Jacobson et al., 1977). The 4880-Å line of the argon laser was used to excite fluorescence from the probes used in this study. For all of these measurements, a 10× objective was used to provide a spot diameter ($2w_s$) of about 8.6 μm, as determined by calculations described earlier (Jacobson et al., 1977). The spot size was verified by the flow calibration scheme of Axelrod et al. (1976) with a diI-C_{16}(3) dried thin-fluorescent film in which the probe is immobilized (M. Schneider and W. W. Webb, personal communication). However, instead of translating the bleached hole across the measuring beam at constant velocity, the bleached hole was moved by using a differential micrometer until half of the initial fluorescence level (prior to bleach) was regained. At this point, the distance translated is $w_s\gamma_F$ where γ_F depends on the extent of bleaching (Axelrod et al., 1976). In general, the hole was found to be asymmetric, a fact we attribute to a displacement of the measuring beam with respect to the bleaching beam (Barisas, 1980). However, this shift was generally less than $0.3w_s$, so that this effect should not introduce more than 10% error in D (Barisas, 1980). Repeated determinations of the sum of w_s measured in one direction (w_s') plus w_s measured in the opposite direction (w_s'') gave a mean value for the beam diameter, ($w_s' + w_s''$), of 8.4 ± 0.7 μm, within experimental error of the calculated value. For achievement of shorter bleach times a high-speed camera shutter (Vincent Associates, Inc., Rochester, NY) was used as the beam flag [BF; see Jacobson et al., (1977)], enabling bleach times of 10 ms to be obtained.

The FRAP data were analyzed as previously described (Wu et al., 1977). In addition, models of one-component diffusion, based on the formulations of Axelrod et al. (1976), and two-component diffusion were employed to computer curve fit selected FRAP data (Z. Derzko, unpublished results). The two-component model has two independently isotropically diffusing populations (D_F, fraction f_F, and D_S, fraction $f_S = 1 - f_F$) which are assumed to have the same bleaching behavior. The computer program also evaluates the "percent fit" and gives confidence limits for the fitted parameters assuming a 95% significance level.

Bleaching Control Studies. It is natural to assume that the photochemistry involved in photobleaching will vary with the chromophore employed. Depending on their photostability, different fluorescent lipid analogues have to be bleached with different doses (intensity × bleach time) in order to obtain enough bleaching to make the measurement; sufficient bleaching means having a small enough F_0/F_i such that the FRAP curve can be discerned (F_i and F_0 are the prebleach and postbleach (at time zero) intensities, respectively). In particular, it was found that the indocarbocyanaine dyes, diI-C_n(3), are hardest to bleach, followed by the oxacarbocyanines, diO-C_n(3), NBD-PE, and, last, the fatty acid probes. NBD-lysoPE displayed considerably greater photostability in the fluid phase than in the gel state.

The question then arises how much photobleaching differences will affect comparisons of the lateral diffusion rates obtained for the various lipid analogues. We have approached this question empirically. In general, we found that increasing bleach intensity (I_B) and bleach time (T_B) causes the value of recovery half-time ($\tau_{1/2}$) to increase; however, control experiments showed that for the ranges of bleach intensities (1–25 mW) and bleach times (10–70 ms) used for this study, $\tau_{1/2}$ did not increase by more than 20%. The maximum bleach times employed satisfied the inequality $T_B \leq 0.1\tau_{1/2}$ which approximately preserves the initial condition calculated in the treatment of Axelrod et al. (1976). The relative independence of $\tau_{1/2}$ on T_B or I_B held in spite of the fact that, typically, plots

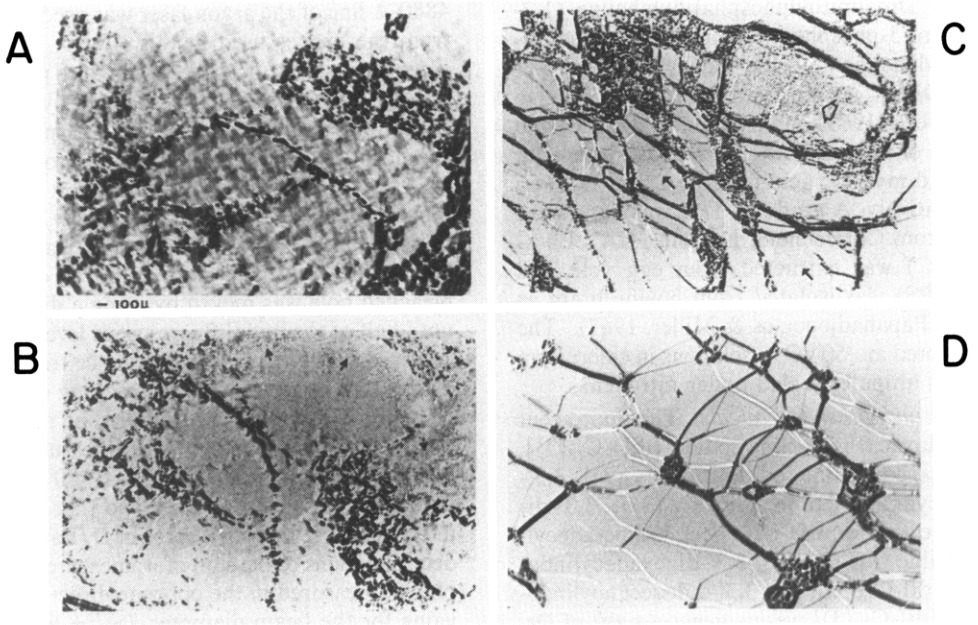

FIGURE 1: Typical morphology of gel-phase DMPC multibilayers approaching a phase transition. (A) Crossed polarized micrograph of DMPC multibilayers at approximately 2 °C (below pretransition) displaying "checkerboarding" as described in the text. Bar represents 100 μm in all micrographs. (B) same field of view as in (A) at a temperature of 12.9 °C (just above the pretransition) but rotated 50° clockwise, showing a decrease in contrast of the "checkerboarding" effect, a general increase in "sawtooth rippling" of the domain boundaries and the appearance of "pebbling" (arrows). (C) Another view of DMPC multibilayers at approximately 23 °C (just below the main phase transition temperature) showing "pebbling" (large arrow) and the appearance of linear defects (dark arrows), which are distinct from the more prominent domain boundaries in that these defects are seen only in the gel state of the multilayers. (D) DMPC multibilayers at (24 °C) showing characteristic appearance of the fluid state. These structures are ~1.5–3.0 μm thick based on height differences observed in focusing on the top and bottom surfaces of the multibilayer.

of K vs. T_B or I_B for two representative probes (diI-C_{18}(3) and F-C_{16}) in fluid DMPC bilayers can be approximated as biphasic linear plots going through the origin in which the linear phase near the origin has a steeper positive slope than that of the next phase at greater T_B or I_B values. Recall that K is related to the postbleach (F_0) and prebleach (F_i) values by $F_0/F_i = K^{-1}(1 - e^{-K})$ and that a simple first-order bleach law predicts that K should be proportional to T_B or I_B (Axelrod et al., 1976). Nevertheless, we assume that because we photobleached all the analogues listed here in the range where $\tau_{1/2}$ values were relatively independent of the bleaching dose, our comparisons of diffusion coefficients are valid.

Results and Discussion

Morphological Observations of the Gel to Liquid-Crystalline Transition. Observing hydrated lipid multibilayers in the polarizing microscope or utilizing the techniques of conoscopy enables one to visualize the optical anisotropy or birefringence of lamellar lipid phases (Powers & Pershan, 1977; Wu et al., 1977; Asher & Pershan, 1979). Under crossed polars, the bright "domain boundaries" of the multibilayers contrast strongly with the darker homogeneous "domains" or "blocks" which are suitable for FRAP (Wu et al., 1977). Further, the fully hydrated multibilayer exhibits morphological characteristics quite typical of the gel or liquid-crystalline state. In the gel state of DMPC bilayers below the pretransition, the domains typically display a "checkerboarding" pattern (Figure 1A). As the temperature is raised to a point just above the pretransition (Figure 1B), the domain boundaries "zigzag", the "checkerboarding" fades in contrast somewhat, and some of the domains take on a pebbly appearance (arrows). Raising the temperature (Figure 1C) further causes the disappearance of "checkerboarding", stronger pebbling of some domains (large arrow), and the appearance of a pronounced linear defect network (small arrows) within domains. These "pebbling" and linear defect features are also seen in gel-state ($T < 8$ °C) PS and gel-state ($T < 41.5$ °C) DPPC multibilayers. The defects invariably disappear as soon as the domains become fluid (Figure 1D). Cycling through the main transition temperature at a rapid rate usually results in an absence of most of the characteristics mentioned, with the exception of the linear defects, which always reappear below T_m. The polarizing microscope images of both DMPC and PS domains illustrating "checkerboarding" and "pebbly" patterns below T_m were correlated with a nonuniform distribution of fluorescence in these regions (photographs not shown). Conversely, above T_m when polarizing images showed homogeneity in the domain structure, the fluorescence staining patterns were also uniform.

According to these morphological criteria the carbocyanine probes and NBD-lysoPE did not alter the value of T_m in DMPC multibilayers by more than ±0.5 °C. All three of the fatty acid probes employed decreased the apparent T_m by 2–4 °C as defined by the transition from defect-containing domains (Figure 1C) to smooth domains (Figure 1D); however, the actual T_m as determined by differential scanning calorimetry was not depressed significantly (N. Düzgunes, personal communication).

Diffusion in the Liquid-Crystalline State: Dependence on Probe Structure. The temperature dependence of lateral diffusion for several probes in various fluid bilayers is given in panel B of Figures 3–6. A data summary and activation energies for diffusion are presented in Table I. Structures of the probes employed are given in Figure 2.

Figures 3 (panel B) and 4 (panel B) show the temperature dependence of the lateral diffusion coefficient (D) for the probes diI-C_n(3) (n = 18, 16, and 12) and diO-C_n(3) (n = 18, 14, 10, and 6), respectively, in fluid DMPC ($T > 24$ °C) multilayers. The diffusion coefficient of both probe types showed little dependence on the acyl chain length of a given

Table I: Summary of Lateral Diffusion Data[a]

probe	DMPC			EPC			brain PS		
	D(24 °C)	D(38 °C)	E_a	D(14 °C)	D(38 °C)	E_a	D(16 °C)	D(38 °C)	E_a
diO-C_{18}(3)	6.7 ± 0.5	9.2 ± 0.4	4.3 ± 2.6	5.9 ± 0.4	8.9 ± 0.3	3.0 ± 0.8	3.7 ± 0.2	7.8 ± 0.1	5.7 ± 2.3
diO-C_6(3)	8.2 ± 1.0[b]	9.0 ± 0.9	4.0 ± 2.7				3.8 ± 0.3	9.5 ± 0.2	7.2 ± 1.7
diI-C_{18}(3)	8.4 ± 0.7	11.9 ± 0.3	4.6 ± 1.2	6.9 ± 0.4	10.9 ± 0.9	3.6 ± 1.1	3.5 ± 0.3	9.8 ± 1.4	8.1 ± 0.7
diI-C_{12}(3)	5.2 ± 1.1	11.3 ± 0.6	10.2 ± 2.1				2.5 ± 0.1	10.1 ± 0.6	11.4 ± 1.7
NBD-PE	6.3 ± 0.5	9.3 ± 2.0	5.9 ± 1.4	4.4 ± 0.3	10.1 ± 0.4	6.8 ± 0.9			
NBD-PC				4.2 ± 0.2	9.5 ± 0.1	7.0 ± 0.3			
NBD-lysoPE	4.5 ± 1.1	7.9 ± 1.6	7.3 ± 0.5	4.6 ± 0.2	11.8 ± 1.2	7.4 ± 1.1			
NBD-C_{12}	7.2 ± 2.5	18.5 ± 2.4	13.0 ± 6.1	4.7 ± 0.2	11.5 ± 0.8	6.9 ± 0.7			

[a] D is in $cm^2/s \times 10^8$ and uncertainties represent ± one standard deviation about the mean for at least three trials; E_a is in kcal/mol and uncertainties represent minimum and maximum slopes in Arrhenius plots based on uncertainty in the D values. [b] At 33 °C only.

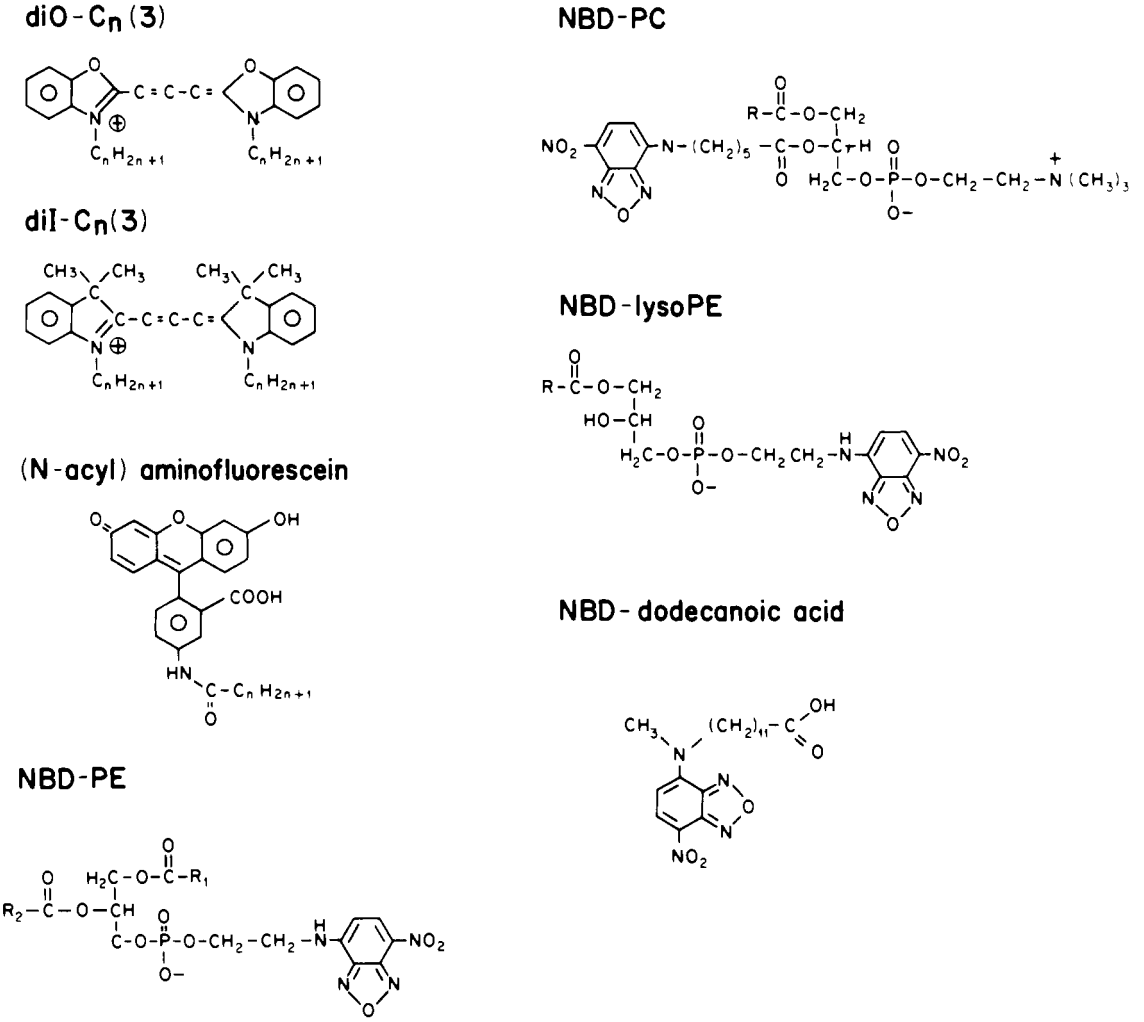

FIGURE 2: Probe structures (going down in left column): diO-C_n(3), 3,3′-diacyloxacarbocyanine; diI-C_n(3), 3,3′-diacylindocarbocyanine; F-C_n, 5-(acylamino)fluorescein; NBD-PE, *N*-(4-nitrobenzo-2-oxa-1,3-diazolyl)phosphatidylethanolamine; NBD-PC, 1-acyl-2-[(*N*-('-nitrobenzo-2-oxa-1,3-diazolyl)amino)caproyl]phosphatidylcholine; NBD-lysoPE, *N*-(4-nitrobenzo-2-oxa-1,3-diazolyl)lysophosphatidylethanolamine; NBD-C_{12}, 12-[methyl(7-nitrobenz-2-oxa-1,3-diazol-4-yl)amino]dodecanoic acid.

probe; all differences were well within experimental error. The similarity of the diI-C_n(3) and diO-C_n(3) diffusion rates in fluid DMPC even down to $n = 6$ indicates that these probes remain anchored to the bilayer.

Figure 5 (panel B) illustrates the temperature dependence of D for three different fluorescent fatty acid probes and a fluorescent lyosphosphatidylethanolamine (NBD-lysoPE). The fatty acid analogues fluorescein palmitate (F-C_{16}) and fluorescein myristate (F-C_{14}) presumably have the fluorescein moiety oriented so that it remains in the vicinity of the head-group region with the hydrocarbon tails embedded in the middle of the membrane bilayer. The third fatty acid probe studied, NBD-C_{12}, consists of a 12-carbon chain with an aromatic fluorescent moiety (NBD) covalently attached to the next-to-last carbon at the end opposite the carboxyl group; its orientation would presumably place the NBD moiety toward the middle of the bilayer. Although the removal of one acyl chain (converting NBD-PE to NBD-lysoPE) did not affect diffusion rates markedly in fluid DMPC, diffusion of the shorter fatty acid analogue, NBD-C_{12}, was more rapid (Table I), especially at the higher temperatures. Note that the activation energy for NBD-C_{12} diffusion is higher than the value typically observed (~13 kcal/mol vs. 4–7 kcal/mol; Table I). This rapid diffusion and high activation energy may either be

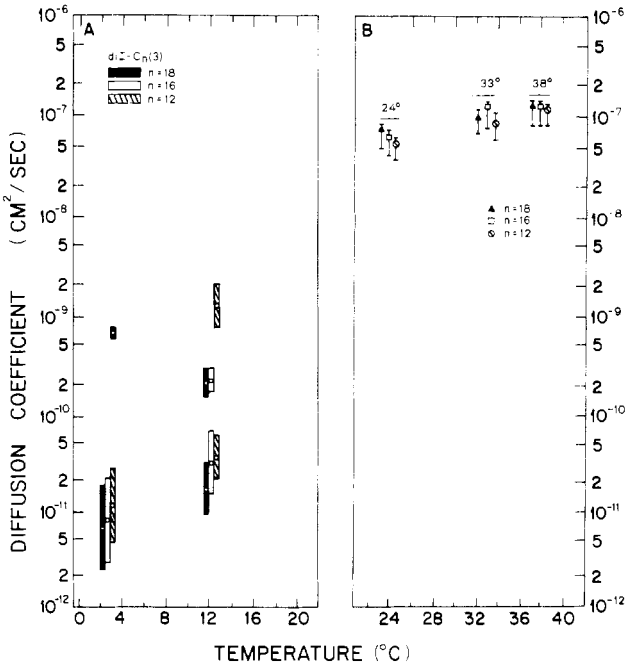

FIGURE 3: Lateral diffusion of the diI-$C_n(3)$ probes in DMPC multibilayers (dye/lipid = 1/9000). Panel A, diffusion as function of temperature below T_m for diI-$C_{18}(3)$ (■), diI-$C_{16}(3)$ (□), and diI-$C_{12}(3)$ (▨). When the FRAP curve was fitted best by two diffusion coefficients, the values are given and the relative lengths of the vertical bar over the slow and fast components give the proportion of these components. *These are not error bars and must not be read logarithmically.* (When f_F or f_S was ≲10%, this component is not shown.) Panel B, diffusion above T_m for diI-$C_{18}(3)$ (▲), diI-$C_{16}(3)$ (□), and diI-$C_{12}(3)$ (⊗). The error bar represents the maximum variation of the value about the average for at least three FRAP trials. Representative FRAP trials were computer fitted, and the resulting 95% confidence limits on D from statistical analyses of the curve fit were found to be about the same as the trial variability illustrated. Representative sample-to-sample variation was similar to the size of the error bars.

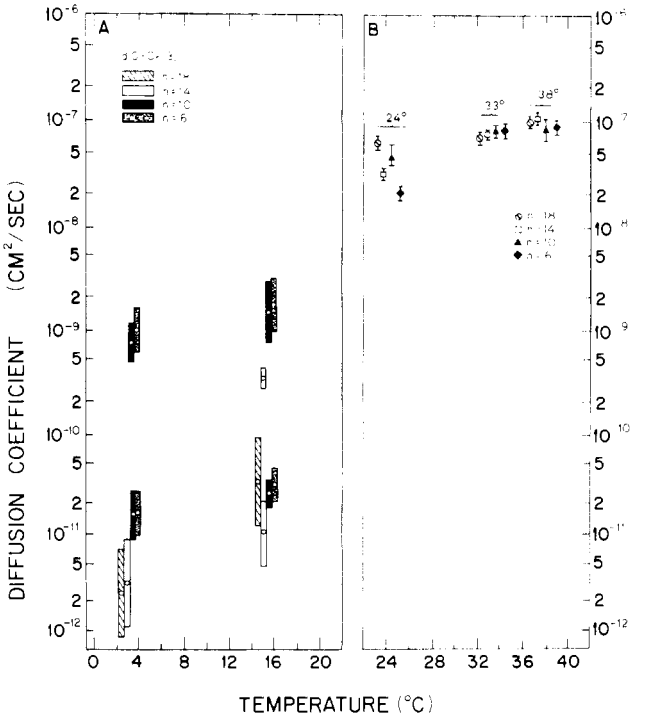

FIGURE 4: Lateral diffusion of the diO-$C_n(3)$ probes in DMPC multibilayers. Panel A, diffusion as a function of temperature below T_m for diO-$C_{18}(3)$ (▨), diO-$C_{14}(3)$ (□), diO-$C_{10}(3)$ (■), and diO-$C_6(3)$ (⊡). Panel B, diffusion above T_m for diO-$C_{18}(3)$ (⊗), diO-$C_{14}(3)$ (□), diO-$C_{10}(3)$ (▲), and diO-$C_6(3)$ (◇). Further details are given in the legend to Figure 3.

characteristic of shorter chain fatty acid diffusion in DMPC bilayers or indicate a propensity for this analogue to undergo dissociation from the bilayer and aqueous diffusion before rebinding to the membrane. However, in EPC multibilayers, this difference was not observed (Table I): all NBD lipid analogues diffused at similar rates with similar temperature dependences.

The results for selected carbocyanine probes in fluid ($T >$ 11 °C) PS multibilayers are given in Figure 6, panel B. At 38 °C, values for D are similar for all the carbocyanine dyes tested in DMPC, EPC, and PS (Table I). Activation energies for diffusion are in the range 4–8 kcal/mol with the exception of slightly lower values for diI-$C_{18}(3)$ and diO-$C_{18}(3)$ in EPC and higher values for diI-$C_{12}(3)$ in PS and DMPC.

The conclusion is that lateral diffusion of the various lipid analogues tested in fluid bilayers is not, in general, an especially sensitive function of (1) the length of the analogue acyl chain, (2) whether the analogue has one or two acyl chains, or (3) the nature of the chromophore. Perhaps this somewhat surprising result can be rationalized by postulating that, provided the probe inserts into the bilayer in an amphipathic manner, its lateral mobility is rate limited by the self-diffusion of the host phospholipid. In this sense, a variety of probes provides at least a relative measure of the lateral self-diffusion coefficient of the phospholipid in the host bilayers.

Diffusion in Different Phospholipid Bilayers. For comparison of the diffusion of a given analogue in different host phospholipid multibilayers, the data should be plotted on a reduced temperature (T_r) scale with $T_r \equiv (T - T_m)/T_m$.

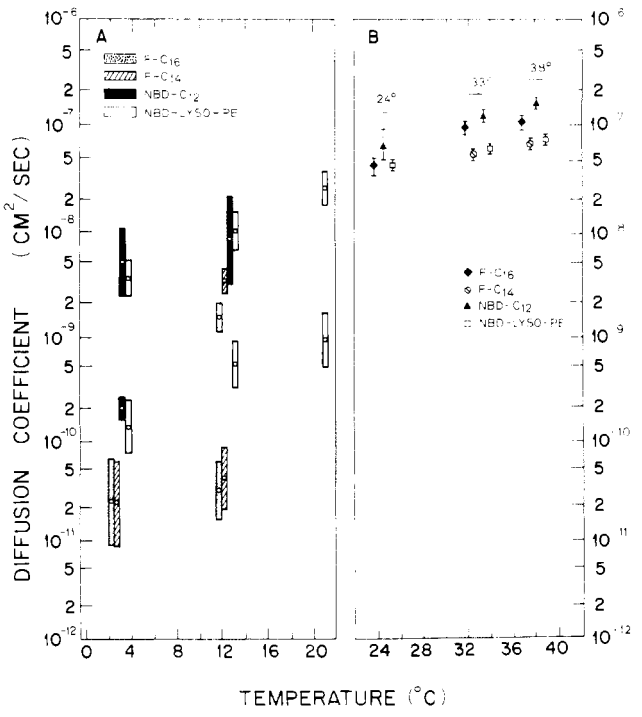

FIGURE 5: Lateral diffusion for single chain fluorescent analogues in DMPC multibilayers. Panel A, diffusion as a function of temperature below T_m for F-C_{16} (⊡), F-C_{14} (▨), NBD-C_{12} (■), and NBD-lysoPE (□). Panel B, diffusion above T_m for F-C_{16} (◇), F-C_{14} (⊗), NBD-C_{12} (▲), and NBD-lysoPE (□). Dye to lipid ratios are 1/10000, 1/100000, 1/10000, and 1/5000, respectively. Further details are given in the legend to Figure 3.

Where necessary, extrapolations and interpolations were done based on the assumption that log $D \propto T_r$. Comparative data are presented in Table II and several trends can be observed. First, the diffusion for those lipid analogues tested at two T_r

Table II: Comparative Lateral Diffusion of Several Probes in Different Lipid Multibilayers at Reduced Temperatures of 0.016 and 0.057[a]

	DMPC reduced temp		DPPC reduced temp		EPC reduced temp		PS reduced temp	
probe	0.016	0.057	0.016	0.057	0.016	0.057	0.016	0.057
diI-C_{18}(3)	8.5	14.8			4.7	5.9	1.9	3.9
diO-C_{18}(3)	6.7	9.6			3.8	4.8	1.4	2.5
diO-C_{12}(3)	7.0	13.9					2.2	4.2
diO-C_6(3)	7.2	9.6					2.9	4.4
NBD-lysoPE	5.2	9.3			1.7	2.8		
NBD-C_{12}	10.2	25.6			2.1	3.2		
NBD-PE	7.1	10.9	16.5		1.6	2.6		
self-diffusion,[b] 20% hydration	3.0	7.5	5	15		~2.0		
maximum hydration			7	18				

[a] Reduced temperature, T_r, is defined as $(T - T_m)/T_m$. T_m was chosen as 24 °C for DMPC, 6 °C for brain PS (Jacobson & Papahadjopoulos, 1975), and −11 °C for EPC (Chapman, 1973). Extrapolations and interpolations are as described in text. (Note that computations of T_r must use absolute temperatures.) [b] Data of Kuo & Wade (1979); approximate D for EPC was obtained by extrapolating data of their Figure 4 to 4 °C. Note that these data are taken at submaximal hydration (20% by weight D_2O).

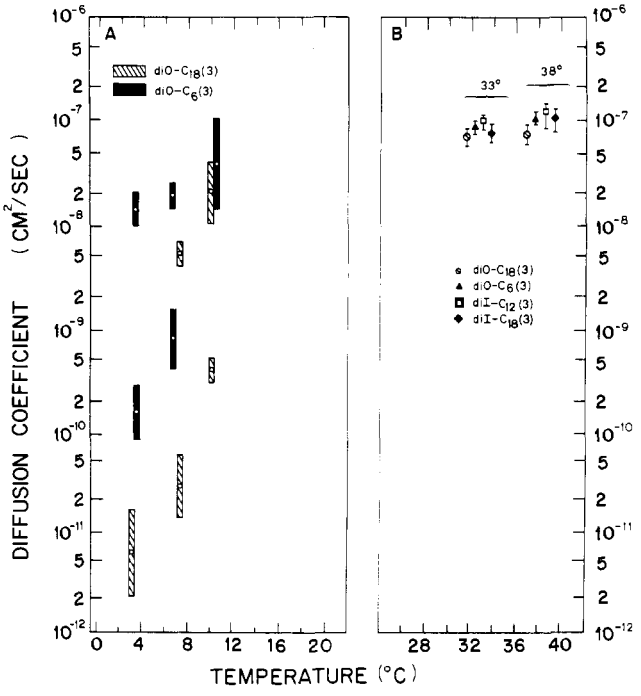

FIGURE 6: Lateral diffusion of carbocyanine dye probes in PS multibilayers at a dye/lipid ratio of 1/9000. Panel A, diffusion as a function of temperature below and within the range of the phase transition for diO-C_{18}(3) (▨) and diO-C_6(3) (■). Data for diI-C_{18}(3) and diI-C_{12}(3) were removed for clarity. Panel B, diffusion above the phase transition for: diI-C_{18}(3) (◇), diI-C_{12}(3) (□), diO-C_{18}(3) (⊘), and diO-C_6(3) (▲). Further details are given in the legend to Figure 3.

values is faster in DMPC and DPPC than in either EPC or PS. This fact is in agreement with the data of Kuo & Wade (1979), showing that self-diffusion in DMPC is more rapid than in EPC at 20% hydration (second last row, Table II). In contrast, comparing either probe diffusion (this work, maximum hydration) or self-diffusion (Kuo & Wade 1979, 20% hydration) in DMPC vs. DPPC at the same T_r value indicates that diffusion increases with increasing chain length of the host bilayer lipids. This surprising result correlates with the fact that, at full hydration, DPPC bilayers are considerably more expanded above T_m than DMPC bilayers (Janiak et al., 1979), having a greater volume per CH_2 group and greater rotameric disorder (Nagle & Wilkinson, 1978).

A second observation is that diffusion is slightly faster, by a nominal factor of 2, in EPC vs. PS bilayers, perhaps reflecting the attraction between the positively charged diI and diO probes and the negative PS molecules (Table II).

Diffusion in the Gel State. In contrast to the liquid-crystalline state, computer curve fitting indicated the presence of two distinct diffusing populations for probes in the gel-state multibilayers in many cases. Two-component diffusion is indicated in panel A of Figures 3–6 as the diffusion coefficient being a double valued function of temperature; thus, a high value (D_F) and low value (D_S) appear; the relative length of the bars around the actual values indicates the fraction of fast (f_F) and slow (f_S) components derived from the computer curve fit. These are mean values based on 2–7 curve fits per temperature point; D_F, D_S, f_F, and f_S do depend on sample history, but, where we have indicated, the two-component nature of the FRAP generally persists. It should also be noted that both D_F and D_S are calculated on the basis of isotropic diffusion; this may not be the appropriate model for either or both of the diffusion components (see below).

Figure 3 (panel A) shows the temperature dependence of the diffusion coefficient of the probe diI-C_n(3) with three different acyl chain lengths (n = 18, 16, and 12) in DMPC for $T < T_m$. As the temperature increases from ~2 °C, the fraction of the fast component increases as the chain length decreases. For example, at ~3 °C, only a slow component ($D \leq 10^{-11}$ cm²/s) is observed for diI-C_{18}(3) and diI-C_{16}(3) while for diI-C_{12}(3), 20% of the population diffuses more rapidly ($5 \times 10^{-10} < D \leq 10 \times 10^{-10}$ cm²/s). At 12 °C, lateral diffusion for diI-C_{12}(3) can be dissected into two approximately equal components with $1 \times 10^{-9} \lesssim D_f \lesssim 2 \times 10^{-9}$ cm²/s and $2 \times 10^{-11} \lesssim D_S \lesssim 7 \times 10^{-11}$ cm²/s. At 12 °C, the other two probes also display a fast component which comprises a smaller fraction of the total probe concentration. In the case of the diI probes, two conditions were found to reduce or eliminate the more rapidly diffusing component. The samples could be aged at 25 °C for up to 2 months or freshly made samples could be equilibrated for 24 h at temperatures below −20 °C. However, neither of these situations is experimentally desirable since, in the first case, degradation of lipid may occur after lengthy aging while, in the second case, there is a large reduction in size of the homogeneous domains, possibly caused by the freezing of water in the samples. The nature of two-component diffusion was not greatly affected by prolonged incubations of the samples at 4 °C, brief sonications below T_m, or repeated "cycling" through the transition temperature, indicating appreciable metastability in the structures responsible for the complex diffusive behavior.

Figure 4 (panel A) shows the temperature dependence of D for the probes diO-C_n(3) having four different acyl chain lengths (n = 18, 14, 10, and 6) in DMPC for $T < T_m$. At ~3 °C, a single slow diffusion coefficient ($D_S \sim 5 \times 10^{-12}$ cm²/s)

was obtained for diO-C_{18}(3) and diO-C_{14}(3). On the other hand, diO-C_{10}(3) and diO-C_6(3) were divided into two approximately equal diffusing populations, one of slower mobility having $D_S \sim 2 \times 10^{-11}$ cm^2/s and a faster component having $D_F \sim 10^{-9}$ cm^2/s. In contrast to the diI probes, raising the temperature to 15 °C did not create an appreciable fast component for diO-C_{18}(3) but merely raised D by an order of magnitude. However, at 15 °C, diO-C_{14}(3) was divided into a minor fast ($D_F \sim 5 \times 10^{-10}$ cm^2/s; $f_F \sim 25\%$) and a major slow ($D_S \sim 10^{-11}$ cm^2/s; $f_S \sim 75\%$) diffusing population. At this temperature, more of both diO-C_{10}(3) and diO-C_6(3) was present as a faster diffusing species ($60\% \leq f_F \leq 70\%$). Note that, as expected, both populations for all probes display a positive temperature coefficient.

Gel-state diffusion of single-chain lipid analogues is seen in Figure 5, panel A. Here some obvious distinctions can be made. NBD-C_{12} and NBD-lysoPE display two-component diffusion with a surprisingly large D_F ($\geq 10^{-9}$ cm^2/s), reaching $\sim 3 \times 10^{-8}$ cm^2/s at 21 °C. For NBD-lysoPE even the slow component was at least an order of magnitude greater than that observed with other probes ($10^{-10} \leq D_S < 10^{-9}$ cm^2/s). The fast component dominates in the case of NBD-C_{12} while for NBD-lysoPE the two populations were approximately equal. On the other hand, F-C_{16} and F-C_{14}, presumably having their bulky chromophores at the membrane surface, display nearly one component, slow diffusion ($D_S \approx 4 \times 10^{-11}$ cm^2/s) at 4 °C, with a small amount of faster component appearing at 12 °C ($D_f \sim 2 \times 10^{-9}$ cm^2/s; $f_F \sim 30\%$).

The lateral diffusion data for the diI and diO probes in PS multibilayers within and just below the broad transition region also indicate some two-component diffusion (Figure 6, panel A). For simplicity, data for the diI probes have been removed. The data show that as the temperature is increased through the transition region the diffusion coefficients for both components increase and that, in general, the proportion of fast component increases. Note that diO-C_{18}(3) is 96% slow component at 4 °C but has become mainly fast component at the upper end of the PS transition (11 °C; Jacobson & Papahadjopulos, 1975). diI-C_{12}(3) and diO-C_6(3) are two component at 4 °C but have become 100% fast component near 11 °C. Finally, it is interesting that diO-C_{18}(3) diffusion at 4 °C is appreciably slower (factor of 40) than the diffusion of diI-C_{12}(3) or diO-C_6(3).

In summary, the simplicity of lipid analogue diffusion rates in fluid bilayers can be contrasted to the more complicated lateral diffusion behavior in gel-state multibilayers. Often, two populations of a given diffusant appear, one of which has a $D \leq 5 \times 10^{-11}$ cm^2/s, and the other $10^{-10} < D \lesssim 10^{-8}$ cm^2/s. The proportion of probe in either fraction depends on the temperature below T_m and on the probe (number and length of acyl chains, chromophore, and its position on the molecule). In general, when two-component diffusion occurs, the D values for both components display a positive temperature coefficient and the fast component grows at the expense of the slow component as the temperature is raised in the gel state. Perhaps the most plausible explanation of this multicomponent diffusion has been offered by Webb and co-workers (personal communication). They have proposed that the slow diffusion ($D \lesssim 10^{-11}$ cm^2/s) corresponds to bulk gel-state diffusion while the more rapid mobility is due to defect-associated diffusion. The latter transport mechanisms could be facilitated, for example, by the linear defects seen in Figure 1. In this view, the partition coefficient describing the distribution of the lipid analogue between the bulk gel-state bilayer and its defect structures would depend on temperature and probe structure; this distribution is then reflected in the proportion of the probe population displaying slow or fast diffusion. It is plausible that the particular fractions of fast and slow components observed would strongly depend on the ability of the bulk gel phase to accept the probe, an impurity molecule. Thus, for example, the rapid diffusion of NBD-C_{12} and NBD-lysoPE could be accounted for because the structure of these probes dictates that they are much more easily accomodated by the gel-state defects where diffusion is more rapid.

Conclusions

Multibilayers undergo a series of morphological alterations, observable in the optical microscope, as they approach and go through the gel to liquid crystalline phase transition temperature. A number of defect structures within the "domains" which appear below T_m disappear above T_m.

Diffusion in the fluid state appears relatively insensitive to the nature of the lipid analogue, its position on the lipid, or to the number or length of the acyl chains on the analogue. With a few exceptions, the activation energy for lateral diffusion of the analogues was 4 kcal/mol $\lesssim E_a \lesssim$ 8 kcal/mol.

For simple saturated phosphatidylcholines in multibilayers, lateral diffusion increases with increasing chain length of the lipid host, while, if shorter saturated lipids are compared to longer chain natural lipids having a more complicated acyl chain composition, lateral diffusion decreases with increasing chain length.

Lateral diffusion in the gel state proceeds, in general, with two rates, a slow process possibly associated with true gel-state diffusion and a faster transport mechanism possibly associated with diffusion along numerous defect structures apparent in gel-state multibilayers. For a particular probe, the proportion of fast and slow component depends upon the structure of the chromophore, the lipid moiety to which it is attached, and the interaction of this analogue with the host bilayer.

Acknowledgments

We gratefully acknowledge the help of Dr. W. L. C. Vaz in the preparation of NBD-lysoPE and the helpful comments of Drs. E.-S. Wu and J. Nagle. We also acknowledge helpful information from Drs. M. Janiak and G. Shipley.

References

Asher, S. A., & Pershan, P. S. (1979) *J. Phys.* (*Orsay, Fr.*) *40*, 161.

Axelrod, D., Koppel, D. E., Schlessinger, J., Elson, E. L., & Webb, W. W. (1976) *Biophys. J. 16*, 1055.

Barisas, B. G. (1980) *Biophys. J. 29*, 545.

Chapman, D. (1973) in *Form and Function of Phospholipids* (Ansell, G. B., Hawthorne, J. N., & Dawson, R. M. C., Eds.) Chapter 6, p 117, BBA Library, Elsevier Amsterdam, London, and New York.

Cherry, R. (1979) *Biochim. Biophys. Acta 559*, 289.

Derzko, Z., & Jacobson, K. (1978) *Biophys. J. 21*, 204a.

Derzko, Z., & Jacobson, K. (1979) *Biophys. J. 25*, 172a.

Fahey, P. F., & Webb, W. W. (1978) *Biochemistry 17*, 3046.

Jacobson, K. (1980) in *Proceedings of NATO Advanced Institute on Lasers in Medicine and Biology*, Plenum Press, New York (in press).

Jacobson, K., & Papahadjopoulos, D. (1975) *Biochemistry 14*, 152.

Jacobson, K., Derzko, Z., Wu, E. S., Hou, Y., & Poste, G. (1977) *J. Supramol. Struct. 5*, 565.

Janiak, M., Small, D., & Shipley, C. G. (1979) *J. Biol. Chem. 254*, 6068.

Kuo, A.-L., & Wade, C. (1979) *Biochemistry 18*, 2301.
Nagle, J., & Wilkinson, J. (1978) *Biophys. J. 23*, 159.
Papahadjopoulos, D., & Miller, N. (1967) *Biochim. Biophys. Acta 135*, 624.
Powers, L., & Pershan, P. S. (1977) *Biophys. J. 20*, 137.
Robles, I. C., & Van Den Berg, D. (1969) *Biochim. Biophys. Acta 187*, 520.
Rubenstein, J., Smith, B., & McConnell, H. M. (1979) *Proc. Natl. Acad. Sci. U.S.A. 76*, 15.
Smith, B. A., & McConnell, H. M. (1978) *Proc. Natl. Acad. Sci. U.S.A. 75*, 2759.
Smith, L. M., Smith, B. A., & McConnell, H. M. (1979) *Biochemistry 18*, 2256.
Vaz, W. L. C., Jacobson, K., Wu, E.-S., & Derzko, Z. (1979) *Proc. Natl. Acad. Sci. U.S.A. 76*, 5645.
Wolf, D. E., Schlessinger, J., Elson, E. L., Webb, W. W., Blumenthal, R., & Henkart, P. (1977) *Biochemistry 16*, 3476.
Wu, E. S., Jacobson, K., & Papahadjopoulos, D. (1977) *Biochemistry 16*, 3936.
Wu, E. S., Jacobson, K., Szoka, R., & Portis, A. (1978) *Biochemistry 17*, 5543.

Effects of Adenosine 5′-Diphosphate on Bovine Glutamate Dehydrogenase: Diethyl Pyrocarbonate Modification†

Alfred George and J. Ellis Bell*

ABSTRACT: Initial rate kinetic studies and reduced coenzyme binding studies with bovine glutamate dehydrogenase have shown that an enzyme–NAD(P)H–glutamate abortive complex is a major participant in the overall enzyme-catalyzed reaction. The allosteric regulator ADP is shown to activate the enzyme by destabilizing this abortive complex. Destabilization of this abortive complex with concomitant activation is also achieved by the ethoxyformylation of a single histidine residue per subunit in the hexameric enzyme. ADP, in addition to its activatory effects, is shown to (a) remove the nonlinearity from the Lineweaver–Burk plots which is attributable to negative cooperativity and (b) inhibit the enzyme as a competitive inhibitor with respect to coenzyme under the appropriate conditions. Ethoxyformylation with diethyl pyrocarbonate, which mimics the activatory effects of ADP, has no effect on the negative cooperativity shown by this enzyme. A model for the action of ADP is proposed in which ADP activates glutamate dehydrogenase by binding to a regulatory binding site and blocks the negative cooperativity by mimicking the natural coenzyme at the active site of the enzyme.

Ox liver glutamate dehydrogenase (EC 1.4.1.3) catalyzes the oxidative deamination of glutamate and a variety of other amino acids (Struck & Sizer, 1960) with either NAD^+ or $NADP^+$ as coenzyme. On the basis of initial rate measurements, Frieden (1959) proposed that each of the six subunits in the glutamate dehydrogenase hexamer had two binding sites for NAD^+ or NADH. Binding of NAD^+ or NADH to the second site produced an activation or an inhibition, respectively, at high concentrations. Since these effects were not observed at high concentrations of the triphosphopyridine nucleotides, which also function as coenzymes, Frieden proposed that the second site was specific for the diphosphopyridine nucleotides. However, more detailed kinetic studies of Engel & Dalziel (1969) demonstrated that the coenzyme activation first observed with NAD^+ as coenzyme (Olson & Anfinsen, 1953) also occurred with $NADP^+$ as coenzyme and that in each case the Lineweaver–Burk plots could be described in terms of a number of linear regions. On the basis of these observations, Dalziel & Engel (1968) proposed that this "coenzyme activation" was due to negative cooperativity. Subsequent studies on the binding of oxidized coenzymes (Egan & Dalziel, 1971) showed no evidence for more than one binding site per polypeptide chain for either NAD^+ or $NADP^+$. In the presence of the substrate analogue glutarate, the data were consistent with either intrinsically nonidentical binding sites or negative homotropic interactions between identical sites in the enzyme–$NAD(P)^+$–glutarate ternary complex. Although the chemical identity of the subunits in the hexamer has been established (Appella & Tomkins, 1966; Smith et al., 1970), there is the possibility that the subunits may be spatially arranged so that they are not in equivalent environments. However, the demonstration that half-saturation of the oligomer with NAD^+ or $NADP^+$ in the presence of glutarate produces a conformational change in the remaining active sites (Bell & Dalziel, 1973) strongly suggests that the nonlinearity found in initial rate studies and in equilibrium binding studies is the result of negative homotropic interactions. This suggestion was substantiated by kinetic studies with thionicotinamide coenzyme analogues (Alex & Bell, 1980).

While many studies [for a review of these, see Dalziel (1975)] have been directed toward establishing the number and types of binding sites for coenzymes and substrates, little attention has been paid to studies of the effects of the nucleotide regulators of glutamate dehydrogenase, ADP and GTP. Previous reports have shown that the binding site for ADP can be covalently modified by the binding site directed affinity label 3′-[*p*-(fluorosulfonyl)benzoyl]adenosine (Pal et al., 1975) which decreases both activation by ADP and the substrate inhibition which is observed at high NADH concentrations, suggesting some overlap of the second NADH binding site and the ADP binding site. We report here the results of initial rate studies, fluorescence binding studies, and chemical modification studies with diethyl pyrocarbonate which allow further definition of the effects of ADP on glutamate dehydrogenase and examine the potential role of the ADP:second NADH binding site in the negative homotropic interactions shown by glutamate dehydrogenase.

† From the Department of Biochemistry, University of Rochester Medical Center, Rochester, New York 14642. *Received June 5, 1980.*

0006-2960/80/0419-6057$01.00/0